

REVIEW

Implication of Water-Rock Interaction for Enhancing Shale Gas Production

Qiuyang Cheng^{1,2,3}, Lijun You^{3,*}, Cheng Chang^{1,2}, Weiyang Xie^{1,2}, Haoran Hu^{1,2} and Xingchen Wang^{1,2}

¹Shale Gas Research Institute, PetroChina Southwest Oil and Gas Field Company, Chengdu, 610056, China

²Sichuan Province Key Laboratory of Shale Gas Evaluation and Exploitation, PetroChina Southwest Oil and Gas Field Company, Chengdu, 610056, China

³State Key Laboratory of Oil and Gas Reservoir Geology and Exploitation, Southwest Petroleum University, Chengdu, 610500, China

*Corresponding Author: Lijun You. Email: youlj0379@126.com

Received: 29 February 2024 Accepted: 07 June 2024 Published: 23 July 2024

ABSTRACT

Horizontal well drilling and multi-stage hydraulic fracturing technologies are at the root of commercial shale gas development and exploitation. During these processes, typically, a large amount of working fluid enters the formation, resulting in widespread water-rock interaction. Deeply understanding such effects is required to optimize the production system. In this study, the mechanisms of water-rock interaction and the associated responses of shale fabric are systematically reviewed for working fluids such as neutral fluids, acid fluids, alkali fluids and oxidative fluids. It is shown that shale is generally rich in water-sensitive components such as clay minerals, acid-sensitive components (like carbonate minerals), alkali-sensitive components (like quartz), oxidative-sensitive components (like organic matter and pyrite), which easily lead to change of rock fabric and mechanical properties owing to water-rock interaction. According to the results, oxidizing acid fluids and oxidizing fracturing fluids should be used to enhance shale gas recovery. This study also indicates that an aspect playing an important role in increasing cumulative gas production is the optimization of the maximum shut-in time based on the change point of the wellhead pressure drop rate. Another important influential factor to be considered is the control of the wellhead pressure considering the stress sensitivity and creep characteristics of the fracture network.

KEYWORDS

Shale gas reservoir; hydraulic fracturing; working fluid; water-rock interaction; oxidation; shut-in; production system

1 Introduction

In organic-rich shale reservoirs with abundant natural gas resources, methane gas resides in both a free state and an adsorbed state in organic matter hosted pores and intercrystalline or intergranular pores among clay minerals [1]. Shale gas output generally goes through a multi-scale transmission including desorption, diffusion, and flow, and production efficiency is very low owing to the slow desorption and diffusion of adsorbed gas and large diffusional and filtrational resistance against free gas in nano-pores [2]. Therefore, commercial shale gas production is achieved through horizontal well drilling and multi-stage hydraulic fracturing of sweet-spot sections to create a flow field with high permeability [3,4].



Physical and chemical reactions usually occur between shale rock and working fluids, such as water-based drilling fluids, alkaline oil-based drilling fluids, slick water, acid fluids, and oxidative gel breakers, in the whole process of economic shale gas production [5]. Water-rock interaction in shale reservoirs may affect borehole stability during drilling, fracturing stimulation performance, shut-in performance and flowback operations. This raises a challenge for well drilling, well hydraulic fracturing, and well management in the context of geology-engineering integration for shale gas development.

Comprehensively understanding the mechanism and characteristics of water-rock interaction in shale gas reservoirs is important to the optimization of working fluid formulas and production systems. Hence, in this study, the interaction mechanisms between shale rock and working fluids commonly used in shale gas wells, as well as the responses of shale fabric to water-rock interaction, are reviewed, and the implications of water-rock interaction for enhancing gas production are discussed.

2 Mechanisms of Water-Rock Interaction in Shale Gas Wells

According to the principles of mineral classification, shale components are classified into three categories: clay minerals, carbonate minerals (including calcite and dolomite), and others (including quartz, pyrite, feldspar, and phosphate) [6]. Clay minerals exposed to water are liable to swell carbonate minerals exposed to acid fluids are liable to dissolve quartzes and clay minerals exposed to alkaline fluids are prone to erode, and organic matter and pyrite tend to settle in a reducing environment, and are apt to be dissolved in an oxygen-rich environment.

2.1 Neutral Fluids

As shown in Table 1, the efficiency of shale components' dissolution by neutral fluids is characterized using a hydrolysis constant, where a small hydrolysis constant indicates a large difficulty of mineral hydrolysis [7]. Ali et al.'s experiments showed indistinct mineral dissolution in shale debris samples (with a particle diameter of ~1 μm) soaked in distilled water for 21 d at 65°C (with a solid-to-liquid ratio of 1 g:5 ml), and these samples exhibited extremely low hydrolysis rates for each mineral component (Table 2) [8].

Table 1: Hydrolysis mechanisms and hydrolysis constants of shale composite minerals

Mineral	Hydrolytic reaction formula	Hydrolysis constant, mol/L
Calcite	$\text{CaCO}_3 (\text{s}) \rightleftharpoons \text{Ca}^{2+} (\text{aq}) + \text{CO}_3^{2-} (\text{aq})$	3.8×10^{-9}
Dolomite	$\text{CaMg}(\text{CO}_3)_2 (\text{s}) \rightleftharpoons \text{Ca}^{2+} (\text{aq}) + 2\text{CO}_3^{2-} (\text{aq}) + \text{Mg}^{2+} (\text{aq})$	10^{-17}
Quartz	$\text{SiO}_2 (\text{s}) \rightarrow \text{HSiO}_3^- (\text{aq}) + \text{H}^+$	$10^{-9.9} - 10^{-11.7}$
Illite	$(\text{K}, \text{H}_3\text{O}, \text{Na}) (\text{Al}, \text{Mg}, \text{Fe})_2 (\text{Si}, \text{Al})_4 (\text{Si}, \text{Al})_4 \text{O}_{10} [(\text{OH})_2, (\text{H}_2\text{O})] \rightleftharpoons \text{K}^+ + \text{Na}^+ + \text{Mg}^{2+} + 2 \sim 68 \text{Al}(\text{OH})^- + \text{H}_4\text{SiO}_4^+ + 4(\text{OH})^-$	$10^{-45.8} - 10^{-73}$
Kaolinite	$\text{Al}_2\text{Si}_2\text{O}_5 (\text{OH})_4 \rightleftharpoons 2\text{Al}^{3+} + 2\text{H}_4\text{SiO}_4 + \text{H}_2\text{O}$	$10^{-37} - 10^{-40}$
Potash feldspar	$3\text{KAlSi}_3\text{O}_8 \rightleftharpoons \text{KAl}_2 (\text{AlSiO}_{10})(\text{OH})_2 + 6\text{SiO}_2 + 2\text{K}^+$	$1.1 \times 10^{-20.04}$
Plagioclase	$5\text{CaAl}_2\text{Si}_2\text{O}_8 + 2\text{H}_2\text{O} \rightleftharpoons 2\text{Ca}_2\text{Al}_3\text{Si}_3\text{O}_{12}(\text{OH}) + \text{CaAl}_4\text{Si}_2\text{O}_{10}(\text{OH})_2 + 2\text{SiO}_2$	$1.1 \times 10^{15} - 2.5 \times 10^{-15}$
Pyrite	$\text{FeS}_2 (\text{s}) + \text{H}_2\text{O} (\text{l}) \rightarrow 4\text{Fe}^{2+} (\text{aq}) + 7\text{S}^{2-} + \text{SO}_4^{2-} (\text{aq}) + 8\text{H}^+$	$10^{-15.2} - 10^{-17.6}$

Table 2: Changes in mineral compositions before and after shale hydrolysis in North America

Shale origin	Type	Mineral content, %												
		Calcite	Dolomite	Quartz	Potash feldspar	Pyrite	Apatite	Zeolite	Gypsum	Smectite	Chlorite	Kaolinite	Illite	Illite/smectite mix-layer
Barnett	Before	0	0	29	0	0	10	0	0.5	5	5	0	33	15
	After	0	0	29	0	0	9	0	0	4	3	0	29	21
Marcellus	Before	5	30	0	0	5	1	0	0.2	0	0	0	19	5
	After	5	30	0	0	5	0	0	0	0	0	0	19	4
Eagle	Before	4	22	0	0	1	0	0	4	0	0	5	0	0
Ford	After	3	21	0	0	0	0	0	0	0	0	5	0	0
Green River	Before	0.4	74	5	4	0	0.6	5	0.4	0	0	0	4	4
	After	0	76	5	4	0	0	5	0	0	0	0	3	4

Shale is rich in clay minerals that comprise illites, illite/smectite mix-layers, chlorites, and kaolinites, and the crystal structures and physical-chemical properties of which determine the strong hydratability of shale rock. Water molecules and hydrated cations are adsorbed and accumulated on the surface of the clay mineral or crystal layers to form an electric double layer, which increases the interlayer repulsion force and interlayer spacing interval and leads to the hydration swelling of clay minerals [9]. Clay hydration is controlled by three main mechanisms: surface hydration, ionic hydration, and osmotic hydration. Surface hydration is initiated by water molecule absorption by clay minerals due to surface hydration energy, ionic hydration refers to the hydration shell forming around compensatory cations on silicate crystals in clay minerals, and osmotic hydration launched after the first two processes is jointly actuated by the repulsion force of the diffuse electric double layer and osmotic pressure [10]. The distance needed to generate surface hydration, which occurs for all clay minerals, is about 1 nm. The distance needed to generate osmotic hydration is larger than 10 nm, and it takes a long time to reach equilibrium due to large volumetric expansion and small swelling pressure [11].

2.2 Alkaline Fluids

Compared to water-based drilling fluids, oil-based drilling fluids with strong anti-pollution capacity and inhibitory capacities can maintain borehole stability and have been widely applied to shale gas wells. To preserve the rheological properties of oil-based drilling fluids and the activities of various treating agents, sodium hydroxide (NaOH) or lime is generally used to adjust the pH value of drilling fluids. The pH value of oil-based drilling fluids is usually higher than 9 [12,13].

Due to high clay content and small clastic mineral particles, shale samples exposed to alkaline fluids are liable to be eroded [12,13]. The corrosion rates of quartz, feldspar, and clay minerals increase with an increasing pH value in an alkaline environment [14]. The corrosion rate of quartz remains unchanged at a pH value of 2.0–8.5 and then sharply increases with the pH value of alkaline fluids; a rise in temperature will also elevate the corrosion rate [15]. Feldspar may react with NaOH solutions at certain concentrations. Alkaline fluids could erode clay minerals, such as kaolinite, smectite, and illite. After erosion, kaolinites will generate amorphous silicon, gibbsite, albites, and analcimes [12]. Table 3 shows complicated and even multi-step associated reaction equations between shale components and alkaline fluids. The intensity of shale mineral erosion by alkaline fluids is ranked as smectite > kaolinite > illite > plagioclase > quartz > orthoclase [16]. The reaction between shale and alkaline fluids mainly generates silicate with some carbonate compounds and hydrated oxides [17]. According to the experiments by Kang et al., the reaction between Longmaxi shale samples from the Sichuan Basin and alkaline fluids is very slow; additionally, they found a positive power correlation between alkaline fluid concentration and reaction rate and a positive exponential correlation between temperature and reaction rate [18].

Table 3: Mechanisms of chemical reactions between shale composite minerals and alkaline fluids

Mineral	Chemical equation
Quartz	$\text{SiO}_2 + \text{NaOH} + \text{H}_2\text{O} = \text{NaH}_3\text{SiO}_4$
Feldspar	$\text{SiO}_2 + 2\text{NaOH} = \text{Na}_2\text{SiO}_3 + \text{H}_2\text{O}$ $\text{Al}_2\text{O}_3 + 2\text{NaOH} = 2\text{NaAlO}_2 + \text{H}_2\text{O}$
Kaolinite	$\text{Al}_2\text{Si}_2\text{O}_5(\text{OH})_4 + 5\text{H}_2\text{O} = 2\text{Al}(\text{OH})_3$ (gibbsite) + $2\text{Si}(\text{OH})_4$ (dissolved silicon) $\text{Al}_2\text{Si}_2\text{O}_5(\text{OH})_4 + 2\text{Na}^+ + 2\text{OH}^- + 4\text{Si}(\text{OH})_4 = 2\text{NaAlSi}_3\text{O}_3$ (albite) + $11\text{H}_2\text{O}$ $\text{Al}_2\text{Si}_2\text{O}_5(\text{OH})_4 + 2\text{Na}^+ + 2\text{OH}^- + 2\text{Si}(\text{OH})_4 = 2\text{NaAlSi}_2\text{O}_6 \cdot \text{H}_2\text{O}$ (analcime) + $5\text{H}_2\text{O}$ $\text{NaAlSi}_3\text{O}_8 + 6\text{OH}^- + 2\text{H}_2\text{O} = \text{Na}^+ + \text{Al}(\text{OH})_4^- + 3\text{H}_2\text{SiO}_4^{2-}$

(Continued)

Table 3 (continued)	
Mineral	Chemical equation
Smectite	$Al_2Si_4O_{10}(OH)_2 + 10H_2O = 2Al(OH)_3$ (gibbsite) + $2Si(OH)_4$ (dissolved silicon) $5Al_2Si_4O_{10}(OH)_2 + 12Na^+ + 2Al(OH)_3 + 12OH^- + 10H_2O = 4Na_3Al_3Si_5O_{16} \cdot 6H_2O$
Illite	$(K, H_3O^+)(Al, Mg, Fe)_2[(Si, Al)_4O_{10}](OH)_2 + OH^- \rightarrow Al(OH)_3 + K^+ + Fe^{2+} + Mg^{2+} + SiO_3^{2-}$ $K_{0.6}Mg_{0.25}Al_{2.3}Si_{3.5}O_{10}(OH)_2 + 3H_2O + 8.7OH^- = 0.6K^+ + 0.25Mg(OH)_2 \downarrow + 2.3Al(OH)_4^- + 3.5H_2SiO_4^{2-}$
Chlorite	$Y_3[Z_4O_{10}](OH)_2 + Y_3(OH)_6 + OH^- \rightarrow Al(OH)_3 + Fe^{2+} + Fe^{3+} + Mg^{2+} + B^{3+} + SiO_3^{2-} + K^+$ (Y—Mg, Al, Fe; Z—Si, Al, Fe ³⁺ , B ³⁺) $Mg_{2.5}Fe_{2.5}Al_2Si_3O_{10}(OH)_8 + 4H_2O + 8OH^- = 2.5 Fe(OH)_2 \downarrow + 2.5Mg(OH)_2 \downarrow + 2Al(OH)_4^- + 3H_2SiO_4^{2-}$
Pyrite	$FeS_2 + 2OH^- \rightarrow Fe(OH)_2 + SO_4^{2-} + 14e^-$ (electrochemical reaction)
Dolomite	$CaMg(CO_3)_2 + 2Na^+ + 2OH^- = CaCO_3 + Mg(OH)_2 + Na_2CO_3$

2.3 Acid Fluids

As a type of working fluid frequently used in reservoir stimulation, acid fluids may erode the microstructure of shale rock directly and initiate various complicated reactions (Table 4). Carbonate minerals exposed to acid fluids show high activity; hydrochloric acid (HCl) reacts quickly with calcites and slowly with dolomites. The reaction experiments at 60°C for individual minerals and acid fluids (pH = 4) showed a calcite reaction rate of 10^{-5} – 10^{-3} mol/m² s and a dolomite reaction rate of 10^{-7} – 10^{-5} mol/m² s [19]. When HCl erodes chlorite crystal layers, the leaching out of Al³⁺, Mg²⁺, and Fe²⁺ ions causes excessive dissolution of chlorites [20], and H⁺ will cause surface dissolution [21]. Surface crystal lattices of kaolinites with almost no isomorphous replacement exhibit extremely high stability in acid fluids and chemically react only with high-concentration (about 21–26%) HCl at high temperatures [22]. The overall structure of illites is destroyed when reacting with HCl, and then, the corroded illites completely peel off from the surface of the shale samples [23]. The products of illite acidification reactions are the primary source of fine migration and could result in pore throat blinding and reservoir permeability decline [24]. In addition, a high-temperature environment facilitates the acid corrosion of illites, chlorites, and albites. Experiments by Black et al. [25] showed an albite reaction rate of $\sim 10^{-10}$ mol/m² s and a clay mineral reaction rate of 10^{-14} – 10^{-10} mol/m² s in acid fluids of pH = 4 at 60°C. The reaction rate of kaolinite or illite is higher than that of chlorite and smectite. Moreover, pyrite is among the common minerals in the sulfide family and could be dissolved effectively in HCl.

Table 4: Mechanisms of chemical reactions between shale composite minerals and acid fluids

Mineral	Chemical equation
Calcite	$CaCO_3 + H^+ = Ca^{2+} + HCO_3^-$
Dolomite	$CaMg(CO_3)_2 + 2H^+ = Ca^{2+} + Mg^{2+} + 2HCO_3^-$
Ankerite	$Ca(Mg, Fe)(CO_3)_2 + 2H^+ = 0.7Fe^{2+} Ca^{2+} + 0.3Mg^{2+} + 2HCO_3^-$
Potash feldspar	$KAlSi_3O_8 + 4H^+ = 2H_2O + K^+ + Al^{3+} + 3SiO_{2(aq)}$
Albite	$NaAlSi_3O_8 + 4H^+ = 2H_2O + Na^+ + Al^{3+} + 3SiO_{2(aq)}$ $NaAlSi_3O_8 + 4H^+ \rightarrow Na^+ + Al^{3+} + 2H_4SiO_4$
Anorthite	$CaAl_2Si_2O_8 + 4H^+ = 4H_2O + 2Ca^{2+} + 2Al^{3+} + 2SiO_{2(aq)}$

(Continued)

Table 4 (continued)	
Mineral	Chemical equation
Kaolinite	$Al_4Si_4O_{10}(OH)_8 + 12HCl_{(aq)} \rightarrow 4Al^{3+} + 12Cl^- + SiO_2 + 10H_2O$
	$Al_2Si_2O_5(OH)_4 + 6H^+ \rightarrow 2Al^{3+} + 2H_4SiO_4 + H_2O$
Illite	$K_{0.6}Mg_{0.25}Al_{2.3}Si_{3.5}O_{10}(OH)_2 + 8H^+ = 0.6K^+ + 0.25Mg^{2+} + 2.3Al^{3+} + 3.5SiO_{2(aq)} + 5H_2O$
	$Illite + H^+ \rightarrow K^+ + Na^+ + Al^{3+} + Fe^{2+} + Fe^{3+} + Mg^{2+} + SiO_2 + H_2O$
Chlorite	$Mg_{2.5}Fe_{2.5}Al_2Si_3O_{10}(OH)_8 + 16H^+ = 2.5Fe^{2+} + 2.5Mg^{2+} + 2Al^{3+} + 3SiO_{2(aq)} + 12H_2O$
	$(Mg^{2+}_{2.8}Fe^{2+}_{1.95})(Si_{2.75}Al_{1.25})O_{10}(OH)_8 + 17H^+ \rightarrow 2.8Mg^{2+} + 1.95Fe^{2+} + 2.5Al^{3+} + H_4SiO_4 + 7H_2O$
	$(Mg^{2+}_{2.5}Fe^{2+}_{2.5})(Si_3Al_2)O_{10}(OH)_8 + 8H^+ = 2.5Mg^{2+} + 2.5Fe^{2+} + 2.5Al^{3+} + 3SiO_{2(aq)} + 8H_2O + 2AlO_2^-$
	$(Mg^{2+}_{4.9}Al_{0.7}Fe^{2+}_{0.1}Fe^{3+}_{0.1})(Si_{3.5}Al_{0.5})O_{10}(OH)_8 + 2H^+ \rightarrow 4.9Mg^{2+} + 12Al^{3+} + 0.1Fe^{2+} + 0.1Fe^{3+} + 3.5H_4SiO_4 + 4H_2O$
Pyrite	$FeS_2 + 2HCl \rightarrow Fe^{3+} + 2Cl^- + H_2S$

2.4 Oxidative Fluids

When black shale formations are tectonically uplifted to crop out, the chemical equilibrium of organic matter and pyrite occurrence is upset due to rising oxidation-reduction potential; hence, oxygenolysis reactions can easily occur in oxygen-rich surface water [26]. Acid water usually generated in the oxidative dissolution of organic matter or pyrite, may corrode carbonate minerals and cause metallic cations to leach out of feldspar, illites, and chlorites and could cause hydrolysis of silicate minerals. It is hard to decompose quartzes in acid and oxidative environments [27]. As shown in Table 5, which compares black shale component stabilities in the land surface environment, organic matter and pyrite are the major objects of weathering and oxidation.

Table 5: Shale component oxidative stabilities and weathering mechanisms

Component type	Component name	Weathering stability	Type of chemical reaction	Major chemical reaction in weathering
Reducing component	Kerogen (C)	Unstable	Oxidation	$C + H_2O + O_2 \rightarrow CO_3^{2-} + 2H^+$
	Pyrite	Unstable	Oxidation	$FeS_2 + 3.5O_2 + H_2O \rightarrow Fe^{2+} + 2SO_4^{2-} + 2H^+$
				$Fe^{2+} + 0.25O_2 + H^+ \rightarrow Fe^{3+} + 0.5H_2O$
Carbonate mineral	Siderite	Unstable	Dissolution and Oxidation	$FeCO_3 + 2H^+ \rightarrow Fe^{2+} + CO_2 + H_2O$
				$Fe^{2+} + 0.25O_2 + H^+ \rightarrow Fe^{3+} + 0.5H_2O$
Carbonate mineral	Calcite	Unstable	Dissolution	$CaCO_3 + 2H^+ \rightarrow Ca^{2+} + CO_2 + H_2O$
	Dolomite	Unstable	Dissolution	$CaMg(CO_3)_2 + 4H^+ \rightarrow Ca^{2+} + Mg^{2+} + 2CO_2 + 2H_2O$
Silicate mineral	Feldspar	Sub-stable	Hydrolysis	Feldspar \rightarrow kaolinite
	Clay mineral	Sub-stable	Hydrolysis	Illite \rightarrow vermiculite and chlorite \rightarrow vermiculite \rightarrow kaolinite + oxide or hydrated oxide of iron
Other	Quartz	Stable	/	/

Oxidizing agents such as hydrogen peroxide (H_2O_2), ammonium persulfate ($\text{Na}_2\text{S}_2\text{O}_8$), and chlorine dioxide (ClO_2) have been widely used in well drilling, well completion, stimulation, and enhanced recovery [28–30]. Experiments by Mikutta et al. [31] revealed the dissolution of organic matter in the soil by H_2O_2 , $\text{Na}_2\text{S}_2\text{O}_8$ and sodium hypochlorite (NaClO) solutions. Oxidative degradation of organic matter in coals accompanies decarboxylation and then the generation of olefin. As the degree of oxidation increases, decarboxylation and ring-opening reactions arise in turn [32]. Some experiments have confirmed the dissolution of organic matter, epyrite, and carbonate minerals in shale by $\text{NaClO}/\text{H}_2\text{O}_2$ [33,34]. In the oxidation process of pyrite by H_2O_2 molecules, thiosulfates (e.g., $\text{S}_2\text{O}_2^{2-}$ and $\text{S}_2\text{O}_3^{2-}$) are produced first and are then oxidized to generate sulfates or are decomposed into elementary sulfurs and bisulfites [35]. There is a power correlation between the oxidation reaction rate of shale rock and H_2O_2 solution concentration and an exponential correlation between the reaction rate and temperature. For an H_2O_2 solution with a mass concentration ranging from 2–10%, the oxidation activation energy of Longmaxi shale samples ranges from 3.51–12.10 kJ/mol [36].

3 Responses of Shale Fabric to Water-Rock Interaction

According to the chemical properties of working fluids used in shale gas wells, water-rock interactions can be classified into two categories: non-chemical dissolution and chemical dissolution. The former mainly refers to the interaction between neutral fluids and shale rock. In spite of the extremely low degree of hydrolysis in shale, hydration swelling of clay minerals may give rise to a lot of cracks. The latter includes acid corrosion, alkaline erosion, and oxidative dissolution. Shale rock containing a complicated pore structure comprises organic matter-hosted pores, clay-mineral pores, and intercrystalline pores in brittle minerals. Besides, there are also abundant laminations and microfractures. The distribution of pores and microfractures is closely related to chemically unstable components, such as quartz, carbonate minerals, organic matter, and clay minerals [37].

3.1 Hydration Swelling

The capillary effect in shale rocks and strong hydration swelling after water imbibed into pores and microfractures among mineral particles jointly lead to the generation, propagation, and connection of microfractures and final macroscopic rock failure [38]. According to fracture mechanics, material failure originates in the generation, propagation, and connection of internal microfractures. Tightly cemented shale is rich in microfractures, and swelling stress caused by clay hydration tends to induce stress concentration at the tip of the microfractures. As the swelling stress increases, continuous microfracture propagation causes shale to burst and collapse once the swelling stress exceeds the critical stress at the fracture tip [39–41]. As shown in Fig. 1, non-clay mineral particles on the shale surface may fall off to form inorganic pores with a diameter from several microns to dozens of microns due to water-rock interaction. In addition, microfractures may occur between organic matter and inorganic minerals and inside inorganic minerals [38]. Liang et al. [42] established a shale crack propagation model involving hydration and wettability (capillary effect), and their results showed that hydration has a great impact on the increment of the stress intensity factor and tends to cause crack propagation. Yang established a model for calculating the release rate of mechanical energy at the tip of shale fractures under capillary force, and they quantitatively discussed the mechanical mechanism of subcritical crack growth under capillary force and explained the reason for shale bursts after water imbibition [43].

In situ conditions, inorganic pores that manifest as microfractures among clay mineral and non-clay mineral particles tend to cause hydration damage [44]. Hydration that mainly occurs along the lamination or pre-existing fractures goes through three stages: a stage with enlarged macropores and cracks, a stage with generated fine pores and enlarged macropores and cracks, and a stage with enlarged fine pores, connected macropores and induced cracks that cause hydration-induced fracturing [45]. Due to the combined effect of surface hydration of clay minerals, ionic hydration, and osmotic hydration, micro-

scale hydration damage gradually evolves into macro-scale failure, which is regarded as successive loss of local rock mechanical strength. Hydration damage tends to occur in shale samples with high clay content, when shale fabric may be seriously destroyed over a short period of time [46]. Under high isotropic compressive stress, shale hydration is likely to close microfractures instead of producing new fractures; under low isotropic compressive stress, hydration induces fractures preferentially growing along lamination and reopening or extending pre-existing fractures [47,48]. Compared with isotropic compressive stress, anisotropic compressive stress is liable to produce hydration-induced fractures; the size of the induced fracture geometry and the number of fractures increase with increasing stress anisotropy [49–51].

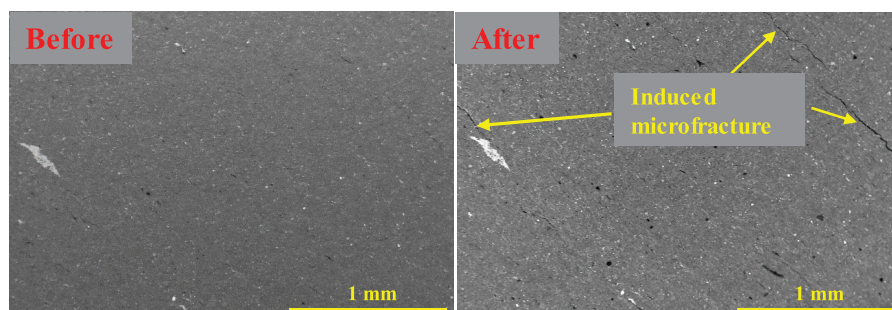


Figure 1: *In situ* field emission scanning electron microscopy (FESEM) observations of Longmaxi shale before and after soaking in distilled water

3.2 Alkaline Erosion

Intense erosion of surface minerals on shale by alkaline fluids may generate many pores (Fig. 2), which increases the internal nano-pore volume and specific surface area, resulting in loosened rock fabric and significantly decreasing rock compression strength. This can consequently expand fractures, enlarge fracture width, and increase the stress sensitivity of shale fractures [18]. As indicated by Kang et al., hydration swelling and alkaline erosion induced by drilling fluid intrusion are the dominant types of shale chemical damage, burst and instability [52]. Since hydroxyl (OH^-) concentration has a great positive effect on the hydration of non-swelling shale rock, alkaline erosion may also accelerate shale hydration swelling. Hydration swelling is intensified when NaOH or potassium hydroxide (KOH) solutions are nearly neutral, alleviated when the pH value ranges from 8 to 9, and enhanced once again when $\text{pH} > 9$ [53]. The hydratability of organic-rich shale increases with pH value; alkaline erosion and its effect on strengthening clay hydration play a role in promoting fracture propagation [54].

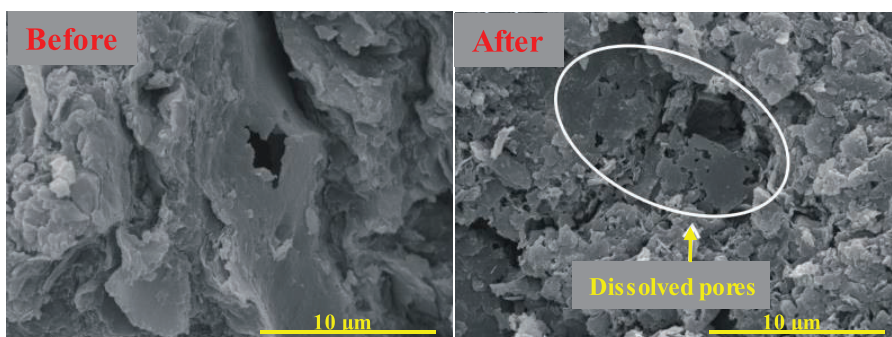


Figure 2: Scanning electron microscopy (SEM) observations of Longmaxi shale before and after soaking in alkaline fluids. Adapted with permission from reference [18], Copyright © 2016, Elsevier B. V

3.3 Acid Corrosion

After treatment of acid fluids, the Bakken shale sample generated mass dissolved pores with the largest diameter of 120 μm , which remarkably improved pore connectivity [55]. Morsy et al. [56] used CT scanning to investigate the porosity change of shale samples acquired from different regions in North America after the acid treatment, in which carbonate-rich shale (Eagle Ford shale) showed a greatly improved porosity after acid corrosion, and clay-rich shale (Barnett shale) showed a negatively growing porosity (Table 6). Three types of microfractures may occur inside shale after acid treatment: stress-induced fractures, acid corrosion-induced fractures, and acidizing-induced contraction fractures. For clay-rich shale, acid corrosion may generate more stress-induced fractures at the boundaries of kaolinites and chlorites/biotites and more acidizing-induced contraction fractures in chlorite zones. For carbonate-rich shale, acid corrosion-induced fractures turn up in zones with anhydrites, calcites, illites, and organic matter [57].

Table 6: Mass loss and porosity change after acid treatment of North American shale

Shale origin	HCl concentration, %	Corrosion rate, %	Original porosity, %	Porosity after acidizing, %	Porosity change, %
Marcellus	0.8	2.06	1.89	2.00	5.82
	1.4	2.32	1.56	1.41	-9.12
	3.0	2.71	2.11	1.29	-38.86
Barnett	0.8	4.51	3.56	2.12	-40.45
	1.4	5.03	5.89	2.59	-56.03
	3.0	9.79	2.44	10.47	329.10
Mancos	0.8	7.73	2.67	3.29	23.22
	1.4	9.79	1.09	2.59	137.61
	3.0	11.86	0.78	2.71	247.44
Eagle Ford	0.8	8.12	1.89	2.71	43.39
	1.4	22.68	0.33	2.00	506.06
	3.0	49.87	1.78	27.29	1433.15

Acid corrosion, which is affected by carbonate mineral distribution, may alter the microstructure of shale rock (Fig. 3), cementing strength of mineral particles, strength of rock mass, and rock deformation and failure [58]. According to the experiments of reactions between Eagle Ford shale samples and dilute hydrochloric acid (HCl) solutions reported by Morsy et al. at 93°C, the elastic moduli of rock samples were reduced by 25–82% after reactions [59]. Decreased shale hardness and microstructure alteration after acid damage are all related to the distribution of reaction minerals [55]. Acid corrosion deteriorates the mechanical strength and breakdown pressure of shale rock, which is favorable for hydraulic fracturing stimulation in shale reservoirs [60].

3.4 Oxidative Dissolution

Outcrop shale weathering mainly works on organic matter and pyrite, and acidulous water produced in the process corrodes carbonate minerals. Due to the erosion by acidulous water, mineral dissolution, generation of secondary minerals, and ion exchange adsorption lead to a change in mineral components and the ways of mineral particle connection, which induces a large number of micropores [61].

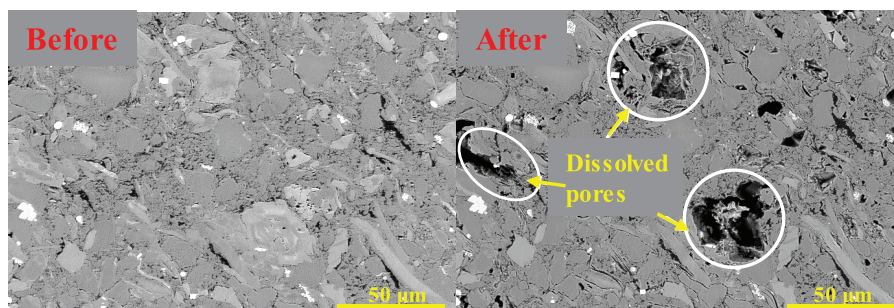


Figure 3: *In situ* FESEM observations of Longmaxi shale before and after soaking in acid fluids

Kuila et al. [62] used low-pressure gas adsorption, X-ray diffraction, rock pyrolysis, and nitrogen adsorption to characterize the pore structures in shale samples from the Silurian System in Eastern Europe, Haynesville, the Paleozoic Erathem and Marcellus in North America, and the Baltic Sea Basin after the treatment with NaClO solutions. After the organic matter in shale rock with high thermal maturities was removed by oxidative dissolution, the volume of pores with diameters smaller than 5 nm was greatly reduced, whereas the volume of pores with diameters greater than 10 nm was greatly increased. Zhu et al. [63] adopted the same methodology to investigate the porosity, total organic carbon (TOC), and mineralogical features of shale samples from the Yanchang Formation in the Ordos Basin in China after treatment with H₂O₂ solutions, and the results showed a positive correlation between a decrease in TOC content and an increase in pore volume.

Chen et al. reported that the average diameter of nano-pores in Longmaxi outcrop shale increased from 4.9 to 24.5 nm after a sufficient reaction with H₂O₂ solutions, the nano-pore volume (with a pore diameter <193.5 nm) increased from 0.025 to 0.041 cm³/g, and the overall pore volume increased from 0.015 to 0.079 cm³/g [33]. Oxidative dissolution may accelerate subcritical crack growth, promote hydration-induced fracturing, and cause oxidative damage to shale rock to intensify macroscopic fracturing under axial stress [64–66]. Fig. 4 shows *in situ* dissolved pores and fractures generated by the oxidative dissolution of pyrite and organic matter [67].

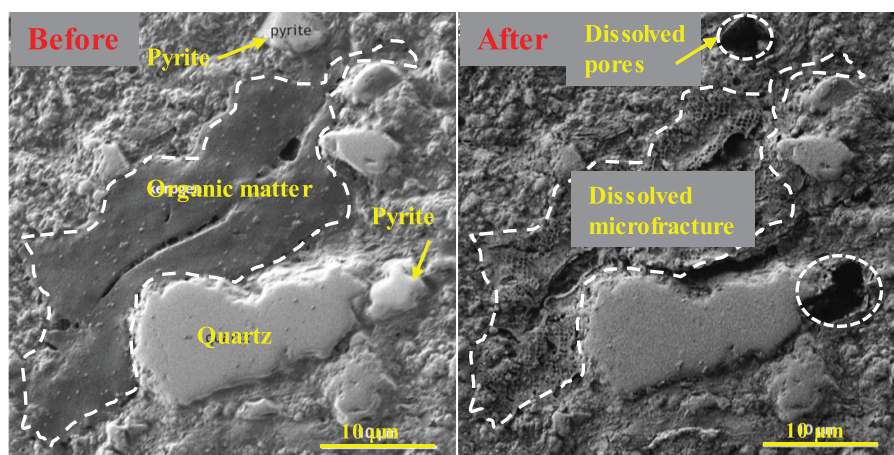


Figure 4: *In situ* SEM observations of shale before and after oxidative dissolution. Adapted with permission from reference [67], Copyright © 2019, ACS Publishing

4 Implications for Enhancing Shale Gas Production

In view of many publications about the mechanisms as well as prevention and control of wellbore instability induced by water-rock interaction [17,52,54,68,69], this study mainly emphasized the improvement of fracturing stimulation and shut-in performance, particularly in terms of the optimization of working fluid formulas and the production system of shale gas wells, to discuss the potential significance of water-rock interaction in enhancing shale gas production.

4.1 Optimization of Working Fluid Formulas

With respect to acid fluids and slick water used in the fracturing stimulation of shale gas wells, this section deals with oxidizing acid fluids, which enhances the performance of acid fluids in reducing the breakdown pressure of shale rock, and with oxidizing fracturing fluids, which facilitates adsorbed gas desorption.

4.1.1 Oxidizing Acid Fluids

To strengthen hydraulic fracturing stimulation, a moderate amount of acid fluids is usually pumped into shale gas wells in advance to corrode carbonate minerals or other types of cement and thus reduce the breakdown pressure of rocks, which is mainly dependent on mineral composition, content, and distribution [64]. According to Eq. (1) (or Eq. (2)) for calculating the breakdown pressure of rocks with vertical (or horizontal) fractures after open hole completion, breakdown pressure is closely related to the porosity at the contact point, Poisson's ratio, and unidirectional tensile strength in the reservoir [70]. Macroscopically, the chemical denudation of minerals impairs the cementing strength of rocks and consequently decreases the cohesive force and the angle of internal friction. Microscopically, microfractures originate in the propagation and connection of mass microfractures under stress.

$$P_{bv} = \frac{3\sigma_H - \sigma_h + \sigma_f - 2\eta P_o}{1 + \phi_c - 2\eta} \quad (1)$$

$$P_{bh} = \frac{P_{ob} + \sigma_f - 2\eta P_o}{\phi_c - 2\eta} \quad (2)$$

$$\eta = \frac{\phi(1 - 2\nu)}{2(1 - \nu)} \quad (3)$$

Here σ_f —unidirectional tensile stress intensity of rocks (MPa);

σ_h and σ_H —horizontal minor principal stress and horizontal major principal stress (MPa);

P_o —pore fluid pressure (MPa);

P_{bv} —vertical fracture actuating pressure (MPa);

P_{bh} —horizontal fracture actuating pressure (MPa);

P_{ob} —burden pressure (MPa);

ϕ_c —porosity at the contact point (%);

ϕ —rock porosity (%);

ν —Poisson's ratio.

For example, Table 7 shows the basic parameters of a shale gas well. Based on porosity change in the process of the oxidative dissolution shown in Table 8, Eq. (1) was used to calculate the breakdown pressure variation corresponding to the generation of a vertical fracture in the shale in the process of oxidative

dissolution (Table 8). It indicates that oxidative dissolution plays an important role in the reduction of breakdown pressure for shale rock. Acid-oxidizing agents, such as H_2O_2 , could coexist with acid fluids, such as dilute HCl. Thus, oxidizing acid fluids (or mixtures of acid fluids and oxidative fluids) are superior to a single acid fluid in reducing the breakdown pressure of shale rock.

Table 7: Basic parameters of a shale gas well in the Sichuan Basin Adapted with permission from reference [71], Copyright © 2015, CNKI Publishing

Parameter	Value	Parameter	Value
Total depth, m	2450	Horizontal major principal stress, MPa	63.5
Vertical stress, MPa	61.50	Horizontal minor principal stress, MPa	47.4
Poisson's ratio	0.25	Pore elasticity	0.9
Tensile strength, MPa	3.50	Pore pressure, MPa	35.7

Table 8: Breakdown pressure of rocks in the process of shale oxidative dissolution (porosity at the contact point originating from reference [33])

Rock sample type	Sample as received	Sample after oxidation treatment for 5 h	Sample after oxidation treatment for 24 h
Porosity at the contact point, %	3.90	10.14	20.54
P_{b0} , MPa	144	135	124

4.1.2 Oxidizing Fracturing Fluids

The statistical data of over 300 wells with pressure-relief production systems using chokes of 1013 mm in the Sichuan Basin showed a quick decline in wellhead pressure and daily gas production. Moreover, these wells did not show a period of stabilized production, and contained two-stage production with early quick decline and late slow decline, corresponding to casing-based production and tubing-based production, respectively. The stage of casing-based production witnessed an initial wellhead pressure of 27 MPa, an annual decline rate of 67%, and the estimated ultimate recovery (EUR) in this stage of 28%. The stage of tubing-based production featured an initial wellhead pressure of 7 MPa, an annual decline rate of 35%, and a EUR of 14%; the additional 58% of EUR can be recovered using other methods.

Regarding the production system, the constant-production reduced-pressure system was implemented at the initial stage of gas well production in this field (the first 2 years), when the production decline rate was high. The constant-pressure reduced-production system was adopted later, with a low production decline rate over a long period of time (Fig. 5). The stage of constant-pressure and reduced-production witnessed cumulative gas production of $6000 \times 10^4 \text{ m}^3$, accounting for 54% of EUR. It indicates that free gas in the fracture network was the major output with relatively high daily production at the initial stage. As the formation pressure dropped quickly, adsorbed gas was rapidly desorbed from the surface of organic matter and released through the fracture network, resulting in a descending decline rate and stable production over a long period at the late stage of production [72]. He et al. examined normal-pressure shale gas production in the Pengshui-Wulong area of Southeastern Chongqing, China, and demonstrated that adsorbed gas output as early as possible may slow down production decline to some extent [73].

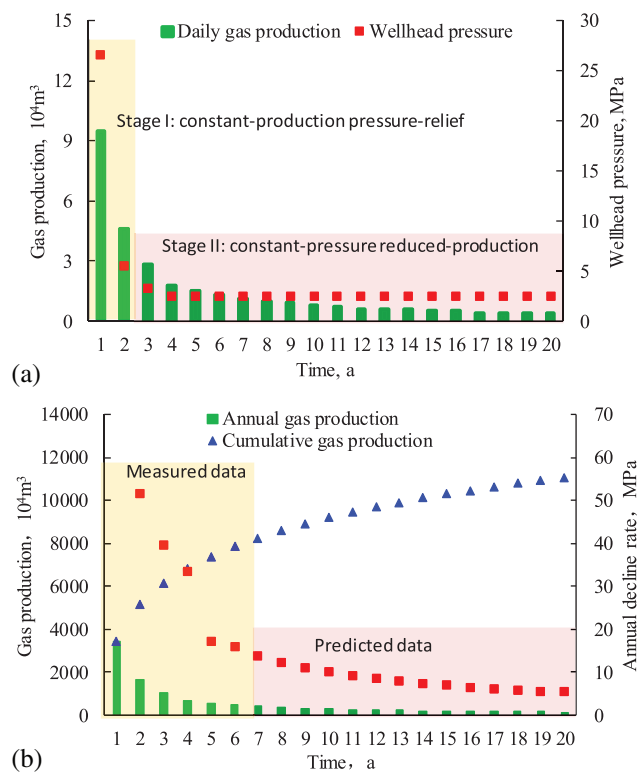


Figure 5: Shale gas production performance from over 300 wells in a field in the Sichuan Basin. (a) Daily gas production and wellhead pressure variations with time; (b) Annual gas production, cumulative gas production, and production decline rate variations with time

Adsorbed gas, with its content accounting for 20%–85% of total gas content in shale, mainly occurs in nano-scale organic matter-hosted pores and inorganic pores with descending adsorptive capacities as organic matter-hosted pores > clay-mineral pores > quartz-hosted pores [74]. Shale samples with high TOC content show a large specific surface area and more sites for the adsorption of methane molecules, for which a linear positive correlation between methane adsorption quantity and TOC content can be found [75]. Adsorbed gas in shale mainly occurs in nano-pores with a diameter <5 nm [62], and organic matter provides more nano-pore volume for adsorbed gas. The structural damage of organic matter molecules and the structural improvement of micron-to nano-scale pores by oxidative dissolution may reduce the methane adsorption quantity in shale. Besides, water film on the pore surface could change the interaction properties of methane adsorption, and water molecules occupy the pore space due to the effect of capillary condensation and consequently decrease the effective specific surface area of methane adsorption [76,77]. That is why wet shale samples show a decreasing methane adsorption quantity [74]. Similar to adsorbed gas substitution by conventional fracturing fluids, oxidative dissolution of organic matter can generate more adsorbed water in shale [78]. Therefore, oxidizing fracturing fluids may promote adsorbed gas desorption and thus enhance shale gas recovery.

With respect to intra-fracture fluid pressure drop due to the filtration of fracturing fluids in shut-in, Yang concluded that water-rock interaction may always contribute to enhanced shut-in performance before intra-fracture fluid pressure falls to the minor principal stress according to simulations of microfracture propagation accelerated by water imbibition in shales [43]. Based on hydration-induced fracturing, oxidizing fracturing fluids will further promote rock fracturing through shut-in and will densify the fracture network.

4.2 Optimization of the Production System

A shale gas well usually goes through three stages after the fracturing operation: shut-in, flowback operations, and production testing. This section deals with the optimization of shut-in time in view of water-rock interaction and pressure-controlled production systems (PCPs).

4.2.1 Shut-In Time

At present, the shut-in time for a shale gas well is established mainly based on two points: proppant flowback control and sustained post-frac stimulation related to rock fracturing induced by water-rock interaction- and formation damage induced by the hydration [79]. In field applications, proppant flowback control usually conforms to the principle of intra-fracture fluid pressure falling below the fracture closing pressure after the termination of pumping; this is the shortest shut-in time. In lab experiments, the longest shut-in time is determined in accordance with the double effects of microscopic reservoir stimulation microfractures and formation damage induced by water-rock interaction.

In shut-in, fracturing fluids spread out along net-like hydraulic fractures, corresponding to intra-fracture fluid pressure attenuation due to fracturing fluid imbibition. The extension of early fracturing fluids from hydraulic fractures to secondary fractures is indicated by a large quick pressure drop, during which rock fracturing induced by water-rock interaction-may densify secondary fractures and increase the space for the water phase. As intra-fracture fluid pressure drops continuously, imbibition-induced fracturing is mitigated gradually. The fluids mainly invade along fracture planes into pores, leading to decreasing efficiency of fluid distribution, which is manifested as a small slow pressure drop. This means that a change point in the pressure drop occurs during the entire process; in other words, the efficiency of imbibition-induced fracturing arrives at a peak (Fig. 6).

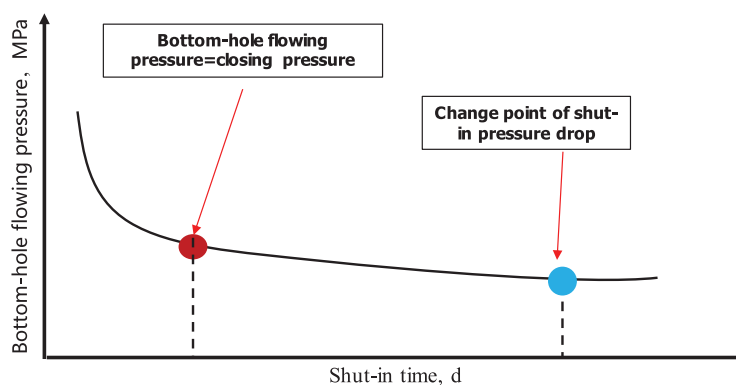


Figure 6: The template to estimate the proper shut-in time of a shale gas well

To validate this viewpoint, wellhead pressure variation with shut-in time was investigated for nine shale gas wells in a field in the Sichuan Basin (Fig. 7a). A change point in the magnitude of the pressure drop can be found. Correspondingly, a change point in the rate of the pressure drop can be found at the same time point according to the derivative of logarithmic wellhead pressure with respect to logarithmic time (Fig. 7b). Shale fracturing induced by water-rock interaction dominates in the time interval before the change point, when a long shut-in time creates more good than harm for shut-in performance. Formation damage dominates in the time interval after the change point, when a longer shut-in time creates more harm than good. Hence, the change point is important for the optimization of the maximum shut-in time.

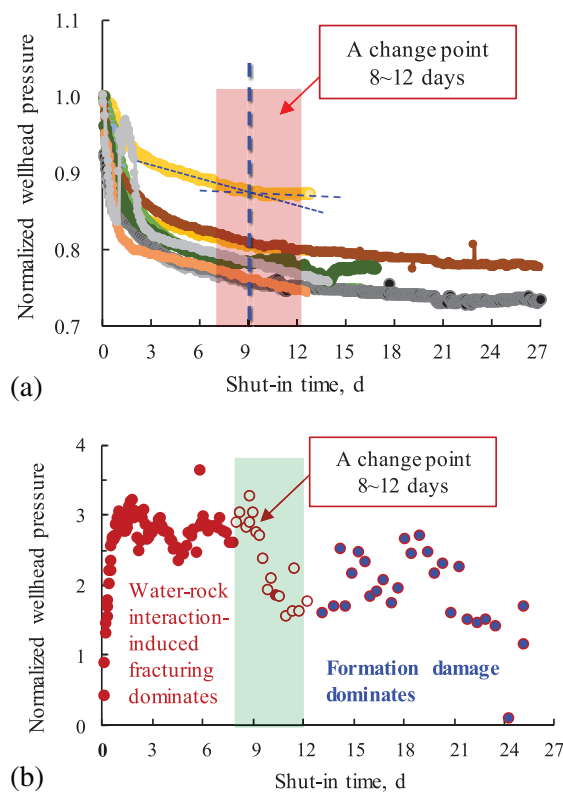


Figure 7: Relationships between wellhead pressure (a) and its derivative (b) and time for nine shale gas wells in the Sichuan Basin

4.2.2 PCPs

For PCPs of a shale gas well, to slow down the decline of fracture conductivity, the production pressure difference usually is increased to the maximum gradually, accompanied by increasing in gas production to a peak and then decreasing gradually [80]. In spite of low daily gas production and cumulative gas production at the initial stage, there is a period of stabilized production with relatively high production to achieve a higher EUR (Fig. 8a) [81]. Similarly, shale gas reservoirs with high formation pressure in the Haynesville Basin in North America show strong stress sensitivity in the fracture network. Using PCPs, the average EUR of shale gas wells in Haynesville is generally elevated by 28% [82].

A complicated hydraulic fracture network may be partially supported by the proppant (proppant-supported fractures or PF), and the others are self-supported with no proppant filled (self-supported fractures or SF). Compared with PF, SF with extremely strong stress sensitivity is easy to close [83]. During increased pressure-difference production with fast pressure relief from major fractures over a short period of time, the pressure sensitivity of fracture networks will result in a dramatic decrease in formation permeability due to the generation of formation damage areas close to the major fractures. It could prevent surrounding gas from moving into major fractures prematurely and thus remarkably decrease gas well production and cumulative production [84,85]. According to the study made by Zhu et al., daily gas production for a single shale well may decrease by 73.5% from reservoirs rich in microfractures and by 39.7% from reservoirs with underdeveloped microfractures owing to stress sensitivity [86]. Moreover, lubrication, hydration, and erosion triggered by the water-rock interaction may aggravate the stress sensitivity of fracture permeability [66,87–89]. Thus, the mechanical strength of shale rock is degraded [90–94], which could seriously harm the conductivity of artificial fractures with the help of stress loading [95–97].

Fig. 8b shows that the effective stress of shale gas reservoirs is relatively low at the early stage of gas well production. If the positive effect of increasing drawdown pressure on increasing production is poorer than the negative effect caused by the stress sensitivity of fracture networks, the drawdown pressure should be limited within a proper range to maintain hydraulic fracture conductivity. It can improve the utilization efficiency of the formation energy to produce gas, and can prolong the period of stabilized production in accordance with the stress sensitivity of fracture networks. At the late stage of gas well production, the effective stress of reservoirs is relatively high. If the effect of increasing drawdown pressure on increasing production is greater than the negative effect caused by the stress sensitivity of fracture networks, the drawdown pressure should be boosted in advance to fully release production, increase potential, and maximize the EUR, in view of the time effect of hydration-induced creep, which may promote fracture closure in shale.

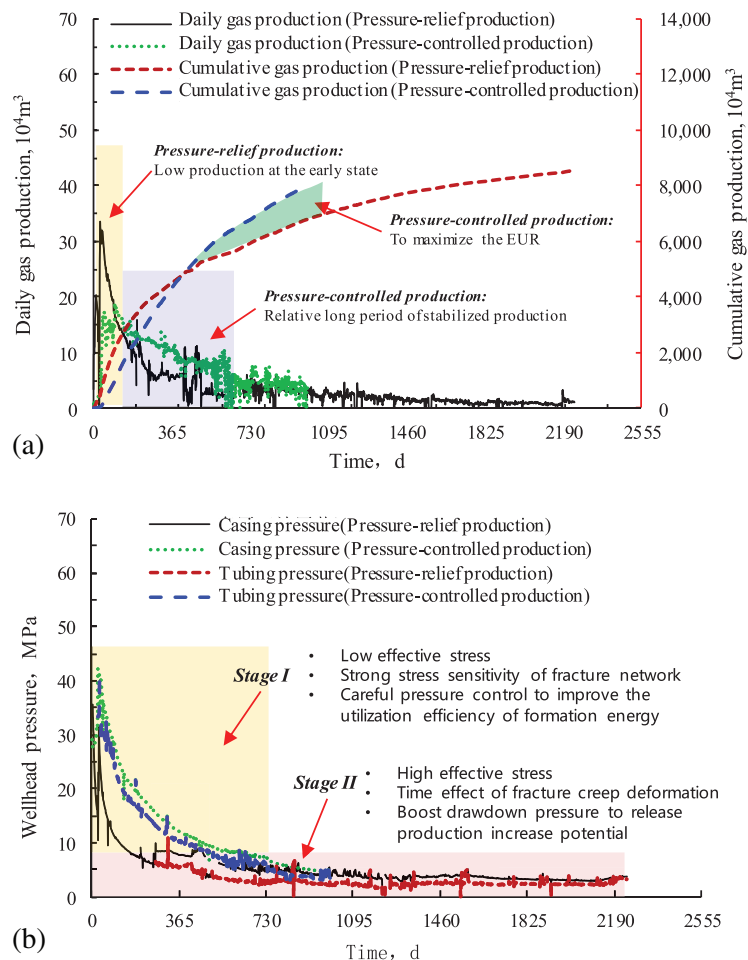


Figure 8: Comparisons between pressure-relief production and pressure-controlled production of shale gas wells in the Sichuan Basin: (a) Casing pressure and tubing pressure. (b) Daily gas production and cumulative gas production

5 Conclusion

In the context of hydraulic fracturing as a current irreplaceable technique and water-rock interaction which is unavoidable in subsurface conditions, understanding how to properly balance and control the double-sided effects of water-rock interaction on increasing production is important to shale gas production, as it both reduces costs and increases benefit. The main conclusions of this study are as follows:

- (1) Shale is rich in water-sensitive clay minerals, acid-sensitive carbonate minerals, alkali-sensitive quartzes, and oxidative-sensitive organic matter and pyrite, and water-rock interaction is liable to change the rock fabric and rock mechanical properties.
- (2) Promoting the application of oxidizing acid fluids and oxidizing fracturing fluids could be favorable for improving hydraulic fracturing and adsorbed gas output and consequently for enhancing shale gas recovery.
- (3) The change points in the magnitude of the pressure drop and the peak time of water imbibition-induced fracturing could be determined through the statistical analysis of the measured shut-in pressure drop of shale gas wells to optimize the shut-in time.
- (4) A PCPs with preserved fracture conductivity is significant to proper pressure control in the whole process of shale gas production, full utilization of producing energy, prolonged period of stabilized production, and EUR maximization.

However, the engineering adaptability of oxidizing acid fluids and oxidizing fracturing fluids needs further demonstration, and PCPs application needs to build a method to design the pressure drop path in production for target wells in the future.

Acknowledgement: This work is supported by the Innovative Research Project for Sichuan Youth Scientific and Technological Innovation and Postdoctoral Research Project of Petrochina Southwest Oil and Gas Field Company.

Funding Statement: Lijun, You, Innovative Research Project for Sichuan Youth Scientific and Technological Innovation (Grants No. 2016TD0016). Qiuyang Cheng, Postdoctoral Research Project of Petrochina Southwest Oil and Gas Field Company (Grants No. 20230304-13).

Author Contributions: The authors confirm contribution to the paper as follows: study conception and design: Qiuyang Cheng & Lijun You; data collection: Weiyang Xie & Haoran Hu; analysis and interpretation of results: Qiuyang Cheng & Cheng Chang; draft manuscript preparation: Qiuyang Cheng & Xingchen Wang. All authors reviewed the results and approved the final version of the manuscript.

Availability of Data and Materials: The data is available from the authors upon reasonable request.

Conflicts of Interest: The authors declare that they have no conflicts of interest to report regarding the present study.

References

1. Curtis JB. Fractured shale-gas systems. *Am Assoc Pet Geol Bull.* 2002;86(11):1921–38.
2. Zhang Y, Zhang B, Liu BH, Liu J, Wei QS, Zhang Q, et al. Status quo and development trends of research on shale gas adsorption and seepage in shale gas reservoirs. *Oil & Gas Geol.* 2024;45(1):256–80.
3. Nie HK, Dang W, Zhang K, Su HK, Ding JH, Li DH, et al. Two decades of shale gas research & development in China: review and prospects. *Nat Gas Indus.* 2024;44(3):20–52.
4. Ma XH, Zhang XW, Xiong W, Liu YY, Gao JL, Yu RZ, et al. Prospects and challenges of shale gas development in China. *Petrol Sci Bul.* 2023;8(04):491–501.

5. Pearce JK, Turner L, Pandey D. Experimental and predicted geochemical shale-water reactions: roseneath and Murteree shales of the Cooper Basin. *Int J Coal Geol.* 2018;187:30–44. doi:10.1016/j.coal.2017.12.008.
6. Jiang YQ, Dong DZ, Lin Q, Shen Y, Chan J, He F. Basic features and evaluation of shale gas reservoirs. *Nat Gas Indu.* 2010;30(10):7–12.
7. Krauskopf K, Bird D. *Introduction to geochemistry.* USA: McGraw-Hill; 1995.
8. Ali M, Hascakir B. Water/rock interaction for Eagle Ford, Marcellus, Green River, and Barnett shale samples and implications for hydraulic-fracturing-fluid engineering. *SPE J.* 2018;22(1):162–71. doi:10.2118/177304-PA.
9. Simpson JP, Dearing HL, Salisbury DP. Downhole simulation cell shows unexpected effects of shale hydration on borehole wall. *SPE Dril Eng.* 1989;4(1):24–30. doi:10.2118/17202-PA.
10. Williams PA, Anderson RL, Ratcliffe I, Greenwell HC, Cliffe S, Coveney PV. Clay swelling—a challenge in the oilfield. *Earth-Sci Review.* 2010;98(3):201–16. doi:10.1016/j.earscirev.2009.11.003.
11. Dachuan L. Review on the study of shale hydration mechanism. *Dril Fluid Compl Fluid.* 1997;14(16):31–3.
12. Mohnot SM, Bae JH, Foley WL. A study of mineral/alkali reactions. *SPE Res Eng.* 1987;2(04):653–63. doi:10.2118/13032-PA.
13. Kang YL, Wu ZJ, Wang JJ. Alkali sensitivity damage: a critical factor causing drastic decrease in oil production for Well Donghe 1 in Tarim Basin. *J Southwest Petrol Uni.* 1997;19(4):14–9.
14. Thomas M. The effect of supplementary cementing materials on alkali-silica reaction: a review. *Cement Concrete Res.* 2011;41(12):1224–31. doi:10.1016/j.cemconres.2010.11.003.
15. Yunfu Z, Wenjie X. *Sedimentary petrology.* Beijing, China: Geological Publishing House Press; 1986. p. 195–220 (In Chinese).
16. Xiong SC. Study on transport law of alkali solution in porous media (Ph.D. Thesis). School of Chinese Academy of Sciences: China; 2009.
17. She JP. Sudden instability mechanism of formation and sealing zone system around shale Wells (Ph.D. Thesis). Southwest Petroleum University: China; 2016.
18. Kang YL, She JP, Zhang H, You LJ, Yu YF, Song MG. Alkali erosion of shale by high-pH fluid: reaction kinetic behaviors and engineering responses. *Nat Gas Sci Eng.* 2016;29(2):201–10. doi:10.1016/j.jngse.2016.01.013.
19. Gonnenthal E, Spyoher N. *Drift-Scale coupled processes (DST and THC seepage) Models.* Las Vegas, NV, USA: Yucca Mountain Project; 2001.
20. Simon DE, Anderson MS. Stability of clay minerals in acid. In: *SPE Formation Damage Control Symposium; 1990; Lafayette: Louisiana.* SPE-19422-MS.
21. Hamer M, Graham RC, Amrhein C, Bozhilov KN. Dissolution of ripidolite (Mg, Fe-chlorite) in organic and inorganic acid solutions. *Soil Sci Soci America.* 2003;67(2):654–61.
22. Gajam SY. Some aspects of hydrochloric acid-leaching of kaolinite clay (Ph.D. Thesis). University of Arizona Campus Repository: USA, 1985.
23. Bibi I, Singh B, Silvester E. Dissolution of illite in saline-acidic solutions at 25°C. *Geo Et Cosmo Acta.* 2011;75(11):3237–49. doi:10.1016/j.gca.2011.03.022.
24. Kamal MS, Mahmoud M, Hanfi M. Clay minerals damage quantification in sandstone rocks using core flooding and NMR. *Petrol Explo Prod Tech.* 2019;9(1):593–603. doi:10.1007/s13202-018-0507-7.
25. Black JR, Carroll SA, Haese RR. Rates of mineral dissolution under CO₂ storage conditions. *Chem Geoy.* 2015;399:134–44. doi:10.1016/j.chemgeo.2014.09.020.
26. Littke R, Klusman U, Krooss B, Leythaeuser D. Quantification of loss of calcite, pyrite, and organic matter due to weathering of toarcian black shale and effects on kerogen and bitumen characteristics. *Geo Et Cosmo Acta.* 1991;55(11):3369–78. doi:10.1016/0016-7037(91)90494-P.
27. Jew AD, Dustin MK, Harrison A, Joe-Wong CM, Thomas DL, Maher K, et al. Impact of organics and carbonates on the oxidation and precipitation of iron during hydraulic fracturing of shale. *Energy Fuel.* 2017;31(7):3643–51.
28. Sanders MP. The application of Oxidative Hydrothermal Dissolution (OHD) to organic-rich shales (Ph.D. Thesis). Southern Illinois University at Carbondale: USA; 2017.

29. Shaun D, Vikas A, Shikha S, Alexandra H. Effect of oxidative breakers on organic matter degradation, contaminant mobility and critical mineral release during shale-fracturing fluid interactions in the Marcellus Shale. *Fuel*. 2023;331(35):125678. doi:10.1016/j.fuel.2022.125678.
30. Zhu J, Zhou J, Yang Z, Xie X, Li X, Li P. Preparation and performance evaluation of microencapsulated acid used for gel breaking of fracturing fluid in low-temperature reservoirs. *J Molec Liquid*. 2024;403:124844–51. doi:10.1016/j.molliq.2024.124844.
31. Mikutta R, Kleber M, Kaiser K, Jahn R. Review: organic matter removal from soils using hydrogen peroxide, sodium hypochlorite, and disodium peroxodisulfate. *Soil Sci Soci America*. 2005;69(1):120–35. doi:10.2136/sssaj2005.0120.
32. Jing Z, Balucan RD, Underschultz JR, Steel KM. Oxidant stimulation for enhancing coal seam permeability: swelling and solubilisation behaviour of unconfined coal particles in oxidants. *Fuel*. 2018;221(8):320–8. doi:10.1016/j.fuel.2018.02.071.
33. Chen Q, Kang Y, You L, Yang P, Zhang X, Cheng Q. Change in composition and pore structure of Longmaxi black shale during oxidative dissolution. *Int J Coal Geol*. 2017;172(4):95–111. doi:10.1016/j.coal.2017.01.011.
34. Cheng QY, You LJ, Kang YL, Zhou Y, Zhang N. An experimental investigation into the oxidative dissolution of typical organic-rich shale from China. *Mar & Petrol Geol*. 2021;130:105117–27. doi:10.1016/j.marpetgeo.2021.105117.
35. Dimitrijevic M, Antonijevic MM, Jankovic Z. Kinetics of pyrite dissolution by hydrogen peroxide in perchloric acid. *Hydrometallurgy*. 1996;42(3):377–86. doi:10.1016/0304-386X(95)00094-W.
36. Cheng QY, You LJ, Kang YL, Zhou Y, Zhang N. Oxidative dissolution kinetics of organic-rich shale by hydrogen peroxide (H₂O₂) and its positive effects on improving fracture conductivity. *Nat Gas Sci Eng*. 2021;89:103875–88. doi:10.1016/j.jngse.2021.103875.
37. Kurotori T, Murugesu MP, Zahasky C, Vega B, Druhan JL, Benson SM. Mixed imbibition controls the advance of wetting fluid in multiscale geological media. *Adv Water Resour*. 2023;175:104429–41. doi:10.1016/j.advwatres.2023.104429.
38. Dou LD. Study on oxygen sensitivity and experimental evaluation method of organic-rich shale reservoirs (Master thesis). Southwest Petroleum University: China; 2019.
39. Wang Y, Liu X, Liang L, Liu XJ, Xiong J. Experimental study on the damage of organic-rich shale during water-shale interaction. *Nat Gas Sci Eng*. 2020;74:103103–17. doi:10.1016/j.jngse.2019.103103.
40. Liu B, Liang Y, Ito T. Numerical study on micro-cracks and permeability changes linked to clay swelling after fracturing in shale rock. *Petrol Sci Eng*. 2022;217:110847–61. doi:10.1016/j.petrol.2022.110847.
41. Li Z, Li G, Li H, Liu JY, Jiang ZJ, Zeng FH. Effects of shale swelling on shale mechanics during shale-liquid interaction. *Energy*. 2023;279:128098–114. doi:10.1016/j.energy.2023.128098.
42. Liang L, Xiong J, Liu X. Experimental study on crack propagation in shale formations considering hydration and wettability. *Nat Gas Sci Eng*. 2015;23:492–9. doi:10.1016/j.jngse.2015.02.032.
43. Bin Y. Study on fracture initiation and expansion behavior of shale induced by water phase imbibition. (Ph.D. Thesis). Southwest Petroleum University: China; 2018.
44. Chen X, Qu X, Xu S, Wang WM, Li S, He H, et al. Dissolution pores in shale and their influence on reservoir quality in Damintun Depression, Bohai Bay Basin, East China: insights from SEM images, N₂ adsorption and fluid-rock interaction experiments. *Mar Petrol Geol*. 2020;117:104394–410. doi:10.1016/j.marpetgeo.2020.104394.
45. Abdullah D, Jagar AA, Mardin A. Exploring the role of hydrophobic nanofluids in reducing shale swelling during drilling: a step towards eco-friendly and sustainable practices. *Coll Surf A: Physicochem Eng Aspects*. 2024;694:134164–78. doi:10.1016/j.colsurfa.2024.134164.
46. Hafiz MA, Tanveer I, Mamdouh A, Muhammad SK. Synergistic effect of polymer and nanoparticles on shale hydration and swelling performance of drilling fluids. *Petrol Sci Eng*. 2021;205:108763–87. doi:10.1016/j.petrol.2021.108763.
47. Zhang S, Sheng JJ. Effect of water imbibition on hydration induced fracture and permeability of shale cores. *Nat Gas Sci Eng*. 2017;45(9):726–37. doi:10.1016/j.jngse.2017.06.008.

48. Zhang S, Sheng JJ. Effects of salinity and confining pressure on hydration-induced fracture propagation and permeability of Mancos shale. *Rock Mech Rock Eng.* 2017;50(11):2955–72. doi:10.1007/s00603-017-1278-z.
49. Zhang S, Sheng JJ. Effect of water imbibition on fracture generation in mancos shale under isotropic and anisotropic stress conditions. *Geo-tech. Geo-Envir Eng.* 2018;144(2):1–10.
50. Liu K, Sheng JJ. Experimental study of the effect of stress anisotropy on fracture propagation in Eagle Ford shale under water imbibition. *Eng Geo.* 2019;249:13–22. doi:10.1016/j.enggeo.2018.12.023.
51. Liu K, Sheng JJ, Zhang Z. A simulation study of the effect of clay swelling on fracture generation and porosity change in shale under stress anisotropy. *Eng Geo.* 2020;278(1–2):105829–45. doi:10.1016/j.enggeo.2020.105829.
52. Kang Y, Chen Q, You L, Lin C, Cheng Q. Laboratory studies of shale fracturing behaviors with rock-drilling fluid interactions. *J China Uni Petrol.* 2016;40(4):81–9 (In Chinese).
53. Wang X, Zhou S. Clay minerals and oil layer protection in sandstone reservoir. China: Geological Publishing House; 1992 (In Chinese).
54. Yu Y. Multi-scale structure description and instability mechanism of organic-rich shale (Ph. D Thesis). Southwest Petroleum University: China; 2013 (In Chinese).
55. Pearce JK, Blach T, Dawson G, Southam G, Paterson DJ, Golding SD. Cooper basin REM gas shales after CO₂ storage or acid reactions: metal mobilisation and methane accessible pore changes. *Int J Coal Geo.* 2023;273(14):104271–90. doi:10.1016/j.coal.2023.104271.
56. Morsy S, Sheng JJ, Hetherington CJ, Soliman MY, Ezewu RO. Impact of matrix acidizing on shale formations. In: *SPE Nigeria Annual International Conference and Exhibition; 2013; Lagos, Nigeria.* SPE-167568-MS.
57. Ogochukwu O, Oladoyin K, Mohamed L, Tobi O, Thomas G, Hallie F, et al. Nano-to macro-scale structural, mineralogical, and mechanical alterations in a shale reservoir induced by exposure to supercritical CO₂. *Appl Energy.* 2022;326:120051–64. doi:10.1016/j.apenergy.2022.120051.
58. Weldu TT, Park D, Jung H, Amini K, Abass H. Effect of dilute acid on hydraulic fracturing of carbonate-rich shale: experimental study. *SPE Pro & Opera.* 2019;34(1):170–84.
59. Morsy S, Hetherington CJ, Sheng JJ. Effect of low-concentration HCl on the mineralogy, physical and mechanical properties, and recovery factors of some shale. *Unconv Oil Gas Res.* 2015;9:94–102.
60. Zeng Y, Chen Z, Bian X. Breakthrough in staged fracturing technology for deep shale gas reservoirs in SE Sichuan Basin and its implications. *Nat Gas Indus.* 2016;36(1):61–7.
61. Bokanda E, Amaya A, Mary E, Florence N, Bisse S, Mokake F. Paleoclimate characteristics of source area weathering and metallogenic implication of cretaceous black shales in the Mamfe basin, (SW Cameroon). *Evidence from Lithochem.* 2023;9:17142–53.
62. Kuila U, McCarty D, Derkowski A, Fischer T, Topór T, Prasad M, et al. Nano-scale texture and porosity of organic matter and clay minerals in organic-rich mudrocks. *Fuel.* 2014;135:359–73. doi:10.1016/j.fuel.2014.06.036.
63. Zhu X, Cai J, Liu W, Lu X. Occurrence of stable and mobile organic matter in the clay-sized fraction of shale: significance for petroleum geology and carbon cycle. *Int J Coal Geol.* 2016;160:1–10. doi:10.1016/j.coal.2016.03.011.
64. Jew A, Druhan J, Ihme M, Kovscek A, Battiato I, Kaszuba J, et al. Chemical and reactive transport processes associated with hydraulic fracturing of unconventional oil/gas shales. *Chem Rev.* 2022;122(9):9198–63. doi:10.1021/acs.chemrev.1c00504.
65. Hull K, Singh S, Crane B, Saini R, AlRuwaili K, AlTammar M, et al. Oxidative hydraulic fracturing fluid to enhance production from source rock reservoirs. *SPE J.* 2024;11(3):1–10. doi:10.2118/221449-PA.
66. Li Y, Yang S, Liu D, Yang C, Yang Z, Li H, et al. Experimental study of shale-fluids interaction during oxidative dissolution with hydrogen peroxide, sodium hypochlorite and sodium persulfate. *Appl Geochem.* 2019;113:104503–12. doi:10.1016/j.apgeochem.2019.104503.
67. Hull KL, Jacobi D, Abousleiman Y. Oxidative kerogen degradation: a potential approach to hydraulic fracturing in unconventional. *Energy Fuel.* 2019;33(6):4758–66. doi:10.1021/acs.energyfuels.9b00104.

68. Horsrud P, Holt RM, Sonstebo EF, Svano G, Bostrom B. Time dependent borehole stability: laboratory studies and numerical simulation of different mechanisms in shale. In: *Rock Mechanics in Petroleum Engineering*; 1994; Delft, Netherlands. SPE-28060-MS.
69. He W, Gomez S, Leonard R, Li D. Shale-fluid interactions and drilling fluid designs. In: *International Petroleum Technology Conference*; 2014; Doha, Qatar. IPTC-17235-MS.
70. Li C. Calculation formula of rock rupture pressure under perforation completion condition. *Oil Drill Prod Tech.* 2002;24(2):37–8.
71. Javed A, Eswaran P, Izhar U, Matthew A. Hydraulic fracturing with low and high viscous injection mediums to investigate net fracture pressure and fracture network in shale of different brittleness index. *Geo Energy Environ.* 2023;33:100416–27.
72. Hamzeh A, Chen N. Long-term production forecast in tight and shale reservoirs: adapting probability density functions for decline curve analysis. *Gas Sci Eng.* 2023;118:205113–24. doi:10.1016/j.jgsce.2023.205113.
73. He X, Zhang P, Fang D, Mei J, He G, Lu B. Production characteristics of normal pressure shale gas in Pengshui-Wulong area, southeast Chongqing. *Petrol Geol Reco Effi.* 2018;25(5):72–9.
74. Alharthy NS, Kobaisi AM, Kazemi H, Graves RM. Physics and modeling of gas flow in shale reservoirs. In: *Abu Dhabi International Petroleum Conference and Exhibition*; 2012; Abu Dhabi. UAESPE-161893-MS
75. Zhu X, Cai J, Wang X, Zhang J, Xu J. Effects of organic components on the relationships between specific surface areas and organic matter in mudrocks. *Int J Coal Geol.* 2014;133:24–34. doi:10.1016/j.coal.2014.08.009.
76. Wang L, Wang D, Cai C, Li C, Zhang N, Yang L, et al. Effect of water occupancy on the excess adsorption of methane in montmorillonites. *Nat Gas Sci Eng.* 2020;80:103393–400. doi:10.1016/j.jngse.2020.103393.
77. Babaei S, Ghasemzadeh H, Tesson S. Methane adsorption of nanocomposite shale in the presence of water: insights from molecular simulations. *Chem Eng J.* 2023;475:146196–11. doi:10.1016/j.cej.2023.146196.
78. Ross D, Bustin RM. Impact of mass balance calculations on adsorption capacities in microporous shale gas reservoirs. *Fuel.* 2007;86(17–18):2696–6.
79. Perera M. A review of underground hydrogen storage in depleted gas reservoirs: insights into various rock-fluid interaction mechanisms and their impact on the process integrity. *Fuel.* 2023;334:126677–89. doi:10.1016/j.fuel.2022.126677.
80. Wang G. Study on optimization method of pressure control production system in shale gas wells in South Sichuan. *Modern Chem Res.* 2022;18:174–6.
81. Jia A, Wei Y, Liu C, Wang J, Li B. A dynamic prediction model of pressure control production performance of shale gas fractured horizontal wells and its application. *Nat Gas Indus.* 2019;39(6):71–80.
82. Unomah GC, Ou L, Panfiloff A, Prasad M. Stress sensitivity of multiscale elastic properties under hydrostatic loading conditions of organic shales at different thermal maturity stages. *Appl Geo.* 2023;209:104906–17.
83. Zhu W, Ma D, Zhu H, An L, Li B. Stress sensitivity of shale gas reservoir and its influence on productivity. *Nat Gas Geo.* 2016;27(5):892–7.
84. Wei Y, Jia A, He D, Wang J, Han P, Jin Y. Comparative analysis of development characteristics and technologies between shale gas and tight gas in China. *Nat Gas Indus.* 2017;37(11):43–52.
85. Zhu W, Ma D. Effective stress characteristics in shale and its effect on pro-ductivity. *Nat Gas Geo.* 2018;29(6):845–52.
86. Jalal F, Amr I, Davood Z, Jalal D. Stress-dependent fluid dynamics of shale gas reservoirs: a pore network modeling approach. *Nat Gas Sci Eng.* 2021;95:104243–52. doi:10.1016/j.jngse.2021.104243.
87. Bandara KMAS, Ranjith PG, Haque A, Wanniarachchi WAM, Zheng W, Rathnaweera TD. An experimental investigation of the effect of long-term, time-dependent proppant embedment on fracture permeability and fracture aperture reduction. *Int J Rock Mech Min Sci.* 2023;161:105299–311.
88. Shoaib M, Runhua F, Muhammad A, Masood A, Ausama G, Alireza K, et al. Mohammad Sarmadivaleh aSupercritical CO₂-Shale interaction induced natural fracture closure: implications for scCO₂ hydraulic fracturing in shales. *Fuel.* 2022;313:122682–93. doi:10.1016/j.fuel.2021.122682.

89. Yang S, Hong W, Wang J, Ranjith P, Wang X. Experimental investigation on the influence of NaCl concentration on triaxial mechanical behaviors of a low-clay shale. *Int J Rock Mech Min Sci.* 2024;176:105716–24. doi:10.1016/j.ijrmms.2024.105716.
90. Huang H, Zhang W, Shi H, Ni J, Ding L, Yang B, et al. Experimental investigation of microscale mechanical alterations in shale induced by fracturing fluid contact. *Gas Sci Eng.* 2024;205264–74.
91. Tan J, Ding Y, Lyu Q, Hu C, Feng G, Yuan Q. Study on the constitutive model and brittleness variations of shale after imbibition in different fracturing fluids. *Geo Energy Environ.* 2023;34:100449–13.
92. Lane R, Aderibigbe A. Rock/fluid chemistry impacts on shale fracture behavior. society of petroleum engineers. In: *SPE International Symposium on Oilfield Chemistry*; 2013 Apr; Texas, USA: The Woodlands. SPE-164102-MS.
93. Antinao Fuentealba FJ, Blanco G, Bianchi LN, Otegui J, Bianchi G. Fracture toughness tests of shale outcrops. *Geoenergy Sci Eng.* 2024;232:212454–544.
94. Katende A, Rutqvist J, Bengte M, Seyedolali A, Bungler A, Puckette J, et al. Convergence of micro-geochemistry and micro-geomechanics towards understanding proppant shale rock interaction: a Caney shale case study in southern Oklahoma, USA. *J Nat Gas Sci Eng.* 2021;96:104296–308. doi:10.1016/j.jngse.2021.104296.
95. Katende A, Awejori G, Bengs M, Nakagawa S, Wang Y, Xiong F, et al. Multidimensional, experimental and modeling evaluation of permeability evolution, the Caney Shale Field Lab, OK, USA. In: *Unconventional Resources Technology Conference*; 2023 Jun 13–15. p. 1505–26.
96. Katende A, Rutqvist J, Massion C, Radonjic M. Experimental flow-through a single fracture with monolayer proppant at reservoir conditions: a case study on Caney Shale, Southwest Oklahoma, USA. *Energy.* 2023;273:127181–92. doi:10.1016/j.energy.2023.127181.
97. Bandara K, Ranjith P, Rathnaweera T. Improved understanding of proppant embedment behavior under reservoir conditions: a review study. *Powder Tech.* 2019;352:170–92. doi:10.1016/j.powtec.2019.04.033.